

USING CLUMPED ISOTOPES AND
RADIOCARBON TO CHARACTERIZE RAPID
CLIMATE CHANGE DURING THE LAST
GLACIAL CYCLE

Thesis by
Nivedita Thiagarajan

In Partial Fulfillment of the Requirements for the degree
of
Doctor of Philosophy



CALIFORNIA INSTITUTE OF TECHNOLOGY
Pasadena, California
2012
(Defended May 18, 2012)

© 2012

Nivedita Thiagarajan
All Rights Reserved

ACKNOWLEDGEMENTS

This thesis is the result of the guidance of my two advisors, Jess Adkins and John Eiler. Their insights and knowledge have always been inspiring for me and they have patiently taught me how to become a scientist.

My scientific discovery was greatly helped by many individuals. John Anderson and Cin-ty Lee at Rice University got me interested in Geology. Aradhna Tripati, Nele Meckler, and Sarah Feakins all guided me at key points early at the start of my graduate career. Ben Passey greatly improved my life (and data) quality by automating the process of making clumped isotope measurements.

I would like to thank the members of NOSAMS at WHOI for teaching me how to make radiocarbon measurements. They are a friendly group and I'll fondly remember my time there.

I also would like to thank Nathan Dallek for patiently helping me isolate hydroxyproline from La brea bones. I could always count on him for support, advice, and good humor.

I'd like to thank the past and present members of the Adkins and Eiler lab for helpful conversations. Alex Gagnon, Weifu Guo, Madeline Miller, Seth Finnegan, Andrea Burke, and James Rae helped me several times dig myself out of whatever deep scientific hole, I'd managed to put myself into. (I'd still be digging it, if it weren't for y'all). I'd also like to acknowledge Daniel Stolper. His enthusiasm for science is infectious and I have enjoyed being contaminated. I'm also grateful to Nami Kitchen for helping me in fiery situations.

Life would not have been the same at Caltech without the good friends I met there. Anne, Anna and I have spent many enjoyable days (without mentioning evenings or nights) at Caltech and away. I'm lucky to have met you. Adam, Guillaume and Katie, y'all have made the time I spent in lab fun.

I'd like to thank Rick Ueda, my photography teacher at the Art Center. I was lucky to take advantage of the photography classes offered at the Art Center, and Rick's kind words helped me at stressful times at work.

I'd like to thank Michael Long for keeping me supplied with fresh eggs, dinners and good spirits when I needed them.

I'd also like to thank my family for always helping me keep my perspective on life.

In memory of Sacrebleu, Le Poisson, and Arraintxu.

ABSTRACT

We generated records of carbonate clumped isotopes and radiocarbon in deep-sea corals to investigate the role of the deep ocean during rapid climate change events. First we calibrated the carbonate clumped isotope thermometer in modern deep-sea corals. We examined 11 specimens of three species of deep-sea corals and one species of a surface coral spanning a total range in growth temperature of 2–25°C. We find that skeletal carbonate from deep-sea corals shows the same relationship of Δ_{47} to temperature as does inorganic calcite. We explore several reasons why the clumped isotope compositions of deep-sea coral skeletons exhibit no evidence of a vital effect despite having large conventional isotopic vital effects.

We also used a new dating technique, called the reconnaissance dating method to investigate the ecological response of deep-sea coral communities in the North Atlantic and Southern Ocean to both glaciation and rapid climate change. We find that the deep-sea coral populations of *D. dianthus* in both the North Atlantic and the Southern Ocean expand at times of rapid climate change. The most important factors for controlling deep-sea coral distributions are likely climatically driven changes in productivity, $[O_2]$ and $[CO_3^{2-}]$.

We take 14 deep-sea corals that we had dated to the Younger Dryas (YD) and Heinrich 1 (H1), two rapid climate change events during the last deglaciation and make U-series dates and measure clumped isotopes in them. We find that temperatures during the YD and H1 are cooler than modern and that H1 exhibits warming with depth. We place our record in the context of atmospheric and marine benthic $\Delta^{14}C$, $\delta^{13}C$, and $\delta^{18}O$ records during the deglaciation to understand the role of the deep North Atlantic during the deglaciation.

We also investigated the role of climate change in the distribution of terrestrial megafauna. To help with this, we also developed a method for compound-specific radiocarbon dating of hydroxyproline extracted from bones in the La Brea Tar Pits. We find that the radiocarbon chronologies of megafauna from several locations around the world, including the La Brea Tar Pits, exhibit an increase in abundance of megafauna during Heinrich events

TABLE OF CONTENTS

Acknowledgements	iii
Abstract.....	iv
Table of Contents	v
List of Figures.....	viii
List of Tables	ix
Chapter I: Introduction	1-1
Chapter II: Carbonate Clumped Isotope Thermometry of Deep-Sea Corals and Implications for Vital Effects.....	2-1
2.1 Abstract.....	2-1
2.2 Introduction.....	2-1
2.3 Methods	2-4
2.4 Results.....	2-5
2.4.i Internal and External Standard Errors	2-9
2.5 Discussion.....	2-9
2.5.i Relationship of Δ_{47} to Temperature	2-9
2.5.ii Vital Effect Mechanisms.....	2-15
2.5.ii.a Vital Effects in Corals	2-15
2.5.ii.b Diffusion.....	2-16
2.5.ii.c Mixing.....	2-18
2.5.ii.d pH	2-21
2.5.ii.e Other Vital Effect Models	2-22
2.6 Conclusions	2-25
2.7 References.....	2-27
Chapter III: Movement of Deep-Sea Coral Populations on Climatic Timescales.....	3-1
3.1 Abstract.....	3-1
3.2 Introduction.....	3-1
3.3 Methods and Materials	3-4
3.3.i Radiocarbon Method	3-4
3.4 Results.....	3-9
3.5 Discussion.....	3-12
3.6 References.....	3-18
Chapter IV: Evidence for the Buildup of the Thermobaric Capacitor in Deep North Atlantic Waters during the Last Deglaciation.....	4-1
4.1 Introduction.....	4-1
4.2 Methods	4-5
4.2.i Radiocarbon Dating Method.....	4-5
4.2.ii U-series Method	4-5
4.2.iii Δ_{47} Method	4-6
4.3 Results.....	4-8
4.4 Discussion.....	4-22
4.5 Conclusions	4-29
4.6 References.....	4-31
Chapter V: Radiocarbon Chronology and the Response of Late Quaternary Megafauna to Rapid Climate Change.....	5-1

5.1 Introduction.....	5-1
5.2 Method Development.....	5-3
5.2.i Extracting Organic Matter from Bones	5-3
5.2.ii Extracting Hydroxyproline from Organic Matter	5-6
5.3 Discussion.....	5-8
5.4 Conclusions	5-22
5.6 References.....	5-24

List of Figures:

<i>Number</i>		<i>Page</i>
2.1	Clumped Isotope Calibration of Deep-Sea Corals.....	2-8
2.2	Internal Standard Error	2-10
2.3	External Standard Error	2-11
2.4	Offsets from Equilibrium in Δ_{47} and $\delta^{18}\text{O}$	2-17
2.5	Vital Effect Mechanisms	2-20
3.1	Age and Depth Distribution of Deep-Sea Corals.....	3-5
3.2	Comparison of Reconnaissance Dating Method with Traditional Method..	3-7
3.3	Radiocarbon Standard Data.....	3-7
3.4	Comparison of Different Radiocarbon Dating Methods	3-8
3.5	YD, ACR, and H1 Profiles	3-10
3.6	Late Holocene Distribution	3-11
3.7	Holocene Distribution.....	3-15
4.1	Ice Core and Marine Reconstructions of Climate Evolution.....	4-2
4.2	Clumped Isotope Cleaning Study.....	4-7
4.3	YD and H1 Temperature and $\Delta^{14}\text{C}$ Profile	4-9
4.4	Vital Effects in Deep-Sea Corals.....	4-21
4.5	Potential Temperature and Salinity for YD and H1	4-23
4.6	Benthic $\Delta^{14}\text{C}$ and $\delta^{13}\text{C}$ over the Deglaciation	4-25
5.1	%C and $\delta^{13}\text{C}$ Results of Cleaning Study	5-5
5.2	$\Delta^{14}\text{C}$ Results of Cleaning Study	5-7
5.3	HPLC Traces of Amino Acid Standard and La Brea	5-9
5.4	Sample Peak Area Calibration	5-10
5.5	Hydroxyproline $\Delta^{14}\text{C}$	5-11
5.6	La Brea Radiocarbon Dates and ECDF	5-12
5.7	Radiocarbon Chronologies of Megafauna Distributions	5-16
5.8	Comparison of Rapid Climate Change Events to Background (by Area) ..	5-17
5.9	Comparison of Rapid Climate Change Events to Background (by Time)..	5-18

List of Tables

2.1 Modern Deep-Sea Coral $\delta^{13}\text{C}$, $\delta^{18}\text{O}$ and Δ_{47} values	2-7
3.1 Radiocarbon and Calendar Ages for North Atlantic Corals	3-22
3.2 Radiocarbon and Calendar Ages for Tasmanian Corals.....	3-24
3.3 Statistical Results Comparing Different Populations	3-28
3.4 Radiocarbon and U-Series Dates for ACR	3-29
4.1 Names and Depths of Corals Analyzed	4-10
4.2 Clumped Isotope Measurements of Corals	4-10
4.3 Individual Clumped Isotope Measurements of Corals and Standards	4-11
4.4 Heated Gas Measurements	4-17
4.5 Corals Displaying VIE in Clumped Isotopes.....	4-19
4.6 ^{14}C Age of Corals.....	4-20
4.7 U-Th of Corals	4-20

Chapter 1

Introduction

The ocean is considered a key parameter during glacial-interglacial transitions and rapid climate change events, as it is one of the largest reservoirs of CO₂ and heat in the atmosphere-climate system. The most common and successful approach to reconstructing past ocean conditions take advantage of isotopic and elemental substitution into foraminiferal CaCO₃ in sediment cores to determine a variety of parameters, including temperature, nutrient ratios, and carbon systematics. Here we develop the use of deep-sea corals as a paleoclimate archive.

Deep-sea corals are a relatively new archive in paleoceanography. Their banded skeletons can be used to generate 100 year high-resolution records without bioturbation. They also have a high concentration of uranium, allowing for accurate independent calendar ages using U-Th systematics. These characteristics make them particularly suited for studying the deep ocean, especially on timescales relevant to rapid climate change. In this work we are interested in understanding the capacity of the ocean to influence rapid climate change. We approach this issue by monitoring and developing new tools to determine deep ocean chemistry recorded in the deep-sea corals.

In Chapter 2, we calibrate the carbonate clumped isotope thermometer in modern deep-sea corals. We examined 11 specimens of three species of deep-sea corals and one species of a surface coral spanning a total range in growth temperature of 2–25°C. Internal standard errors for individual measurements ranged from 0.005‰ to 0.011‰ (average: 0.0074‰) which corresponds to 1–2°C. External standard errors for replicate measurements of Δ_{47} in corals ranged from 0.002‰ to 0.014‰ (average: 0.0072‰) which corresponds to 0.4–2.8°C. This result indicates that deep sea corals can be used for paleothermometry, with precisions as good as 0.4°C. We also observe no vital effects in Δ_{47} for samples that display large vital effects in $\delta^{18}\text{O}$ and $\delta^{13}\text{C}$. We explore several reasons for why the clumped isotope

composition of deep-sea corals exhibit no evidence of a vital effect and conclude that pH effects could explain the observed variations in Δ_{47} and $\delta^{18}\text{O}$.

In chapter 3, we use a new dating technique, called the reconnaissance dating method to investigate the ecological response of deep-sea coral communities in the North Atlantic and Southern Ocean to both glaciation and rapid climate change. We find that the deep-sea coral populations of *D. dianthus* in both the North Atlantic and the Southern Ocean expand at times of rapid climate change. However, during the more stable Last Glacial Maximum the coral population globally retreats to a more restricted depth range. Holocene populations show regional patterns that provide some insight into what causes these dramatic changes in population structure. The most important factors are likely responses to climatically driven changes in productivity, $[\text{O}_2]$ and $[\text{CO}_3^{2-}]$.

In chapter 4, we take advantage of the results of the previous two chapters. We analyze 14 deep-sea corals that we had dated to the Younger Dryas (YD) and Heinrich 1 (H1), using the reconnaissance dating technique and make high-precision radiocarbon dates, U-series dates and clumped isotope measurements. We find that temperatures during the YD and H1 are cooler than modern and that H1 exhibits warming with depth. This warming at depth supports the “Thermobaric Capacitor” hypothesis for causing deep ocean mixing. We place our record in the context of atmospheric and marine benthic $\Delta^{14}\text{C}$, $\delta^{13}\text{C}$ and $\delta^{18}\text{O}$ records during the deglaciation to understand the role of the deep North Atlantic during the deglaciation.

In chapter 5, we investigate the effects of rapid climate change on the terrestrial biosphere, particularly the distribution of terrestrial megafauna. Current hypotheses for the extinction of megafauna focus on human interactions or environmental change. Most of the climate change hypotheses emphasize either changes in habitat or the fast rate of climate change. To further explore the relationship of megafauna to rapid climate change, we examine the abundance of megafauna in the La Brea Tar Pits during the YD and H1.

The La Brea Tar Pits are an exceptionally well preserved archive that has trapped

over three million fossil skeletons including 3400 large mammals. The deposits are a series of open asphalt seeps that have acted as animal traps for at least the past 50,000 years. Previous studies have been limited by weak chronological control, as stratigraphic position is known to be an unreliable indicator of relative age within the asphalt deposits and the asphalt itself has been a large source of carbon contamination. To help with this, we have developed an HPLC method for compound-specific radiocarbon dating of hydroxyproline extracted from bones in the La Brea Tar Pits. We find that in La Brea and other locations around the world, the megafauna abundance actually increases. Therefore megafauna extinctions were either primarily caused by humans, a climatic variable that did not adversely affect megafauna during rapid climate change events, or some combination of the two.

Chapter 2

Carbonate Clumped Isotope Thermometry of Deep-Sea Corals and Implications for Vital Effects

2.1 ABSTRACT

We examined 11 specimens of three species of deep-sea corals and one species of a surface coral spanning a total range in growth temperature of 2–25°C. Analytical precision for individual measurements ranged from 0.005 to 0.011‰ (average: 0.0074‰) which corresponds to ~1 to 2°C. Analytical precision for replicate measurements of Δ_{47} in corals ranged from 0.002 to 0.014‰ (average: 0.0072‰) which corresponds to 0.4 to 2.8°C. We find that skeletal carbonate from deep-sea corals shows the same relationship of Δ_{47} (the measure of ^{13}C - ^{18}O ordering) to temperature as does inorganic calcite. In contrast, the $\delta^{18}\text{O}$ values of these carbonates (measured simultaneously with Δ_{47} for every sample) differ markedly from equilibrium with seawater; i.e., these samples exhibit pronounced ‘vital effects’ in their bulk isotopic compositions. We explore several reasons why the clumped isotope compositions of deep-sea coral skeletons exhibit no evidence of a vital effect despite having large conventional isotopic vital effects.

2.2 INTRODUCTION

Oxygen isotope measurements of biogenic marine carbonates are a long established and important tool for determining past ocean temperatures (Epstein et al., 1953; McCrea, 1950; Urey, 1947). In the decades following its initial development, the $\delta^{18}\text{O}$ thermometer was applied to planktonic foraminifera to reconstruct ocean temperature shifts on glacial/interglacial time scales (Emiliani, 1955). However it was later recognized that the planktonic record reconstructed from foraminifera $\delta^{18}\text{O}$ reflects a combination of the temperature from which the carbonate grew, and global changes in ice volume (Shackleton, 1967).

Deconvolving these two effects on the marine-carbonate oxygen isotope record remains a central problem in paleoclimatology. Chappell and Shackleton (1986) addressed this problem by examining dated coral terraces and benthic $\delta^{18}\text{O}$ records. Previously, the benthic $\delta^{18}\text{O}$ records had been interpreted assuming a constant temperature in the abyssal ocean. However, the resulting ice volume estimates derived from benthic $\delta^{18}\text{O}$ records could not be reconciled with ice volume records derived from the altitudes of dated coral terraces. Chappell and Shackleton (1986) made a detailed comparison of a coral terrace record in the Huon Peninsula with a benthic $\delta^{18}\text{O}$ record from the Pacific Ocean and concluded that during the last interglaciation, abyssal temperatures changed only during the transition from Marine Isotope Stage (MIS) 5e to 5d, and during the last glacial termination.

Subsequent efforts have reconstructed the $\delta^{18}\text{O}$ of the water of the deep ocean during the Last Glacial Maximum based on isotopic analyses of marine pore fluids (Schrag and DePaolo, 1993). Cutler et al. (2003) reconstructed a sea level curve based on fossilized surface corals from the Huon Peninsula and Barbados and combined this new sea level curve with the $\delta^{18}\text{O}$ of the water of the deep ocean reconstruction determined from pore fluids (Adkins et al., 2002). This work established that deep-sea temperatures have warmed by 4°C in the Atlantic and 2°C in the Pacific since the Last Glacial Maximum. In all of these studies, independent estimates of the change in sea level or of the $\delta^{18}\text{O}$ of the water of the deep ocean were necessary to extract deep ocean temperatures from benthic $\delta^{18}\text{O}$ data.

Carbonate clumped isotope thermometry is a new temperature proxy based on the ordering of ^{13}C and ^{18}O atoms into bonds with each other in the same carbonate molecule. The proportion of ^{13}C and ^{18}O atoms that form bonds with each other in a carbonate mineral has an inverse relationship with growth temperature. This isotopic ‘clumping’ phenomenon exists due to a

thermodynamically controlled homogeneous isotope exchange equilibrium in the carbonate mineral (or, perhaps, in the dissolved carbonate-ion population from which the mineral grows). This exchange reaction is independent of the $\delta^{18}\text{O}$ of water and $\delta^{13}\text{C}$ of DIC from which the carbonate grew; therefore it can be applied to settings where these quantities are not known (Eiler et al., 2003; Eiler and Schauble, 2004; Ghosh et al., 2006).

Here we calibrate carbonate clumped isotope thermometry in modern deep-sea corals. Deep-sea corals are a relatively new archive in paleoceanography. Their banded skeletons can be used to generate ~ 100 -year high-resolution records without bioturbation. They also have a high concentration of uranium, allowing for accurate independent calendar ages using U-Th systematics. A thermometer in deep-sea corals could address the phasing of the offset between Northern and Southern Hemisphere in rapid climate events. The Greenland and Antarctic ice cores both show that temperature and CO_2 are tightly coupled over the last several glacial interglacial events. However, the synchronization of the ice cores from the two regions using atmospheric methane concentration trapped in the ice layers revealed that Antarctica warms several thousand years before the abrupt warmings in the Northern Hemisphere (Blunier and Brook, 2001). The deep ocean is a massive heat and carbon reservoir with an appropriate time constant that could be used to explain the several thousand year offset between the hemispheres. A temperature record of the deep ocean that spans the time period of these rapid climate events would help explain the role of the deep ocean in rapid climate change events.

Deep-sea corals are also an important resource to study vital effects because they grow without photosymbionts and grow in a relatively homogeneous environment with minimal variations in temperature and the composition of co-existing water. Therefore, offsets from equilibrium that we observe in any chemical proxies can be attributed to biological processes associated

with calcification. Previous work in surface and deep-sea corals has found evidence of isotopic disequilibrium in $\delta^{13}\text{C}$ and $\delta^{18}\text{O}$ (Adkins et al., 2003; Emiliani et al., 1978; McConaughey, 1989; Weber and Woodhead, 1970; Weber, 1973). McConaughey attributes these offsets in surface corals to kinetic and metabolic effects. However light-induced metabolic effects cannot be invoked to explain offsets in deep-sea corals because they do not have any photosymbionts. Radiocarbon dating of modern corals and their surrounding dissolved inorganic carbon (DIC) also indicate that the skeletal material of deep-sea coral is drawn almost entirely from the ambient inorganic carbon pool and not from respired CO_2 (Adkins et al., 2003). Due to the correlation between growth banding and stable isotopes within individual corals, Adkins et al. (2003) proposed that vital effects in deep-sea corals involve a thermodynamic response to a biologically induced pH gradient in the calcifying region. Watson (2004) proposed a surface entrapment model in which growth rate, diffusivity, and the surface layer thickness all control crystal composition. In this model, the trace element or isotope composition of the crystal is determined by the concentration of that element in the near-surface region and the outcome of the competition between crystal growth and ion migration in the near-surface region.

More recently, Ghosh et al. (2006) found evidence of an anomalous enrichment in Δ_{47} values in winter growth bands in a *Porites* sample from the Red Sea, suggesting that surface corals may have a vital effect in this parameter. Here we look at a variety of deep-sea corals grown from different locations, and analyze their Δ_{47} values to develop a modern calibration for carbonate clumped isotope thermometry and to investigate the mechanisms of vital effects.

2.3 METHODS

Samples examined in this study were obtained from the Smithsonian collection (National Museum of Natural History). We focused on *Desmophyllum* sp., *Caryophyllum* sp., and

Ennalopsammia sp. collected from a variety of locations and depths. One *Porities* sp. coral from the Red Sea was also analyzed. Isotopic measurements were made on pieces from the septal region of the coral that were cut using a dremel tool. For each clumped isotope measurement, eight to fifteen mg from each coral was analyzed. The outsides of the coral were scraped with a Dremel tool to remove any organic crusts. The sample was then digested in 103% anyhydrous phosphoric acid at 25°C overnight. The product CO₂ was extracted and purified using methods described previously (Ghosh et al., 2006).

Evolved CO₂ was analyzed in a dual inlet Finnigan MAT-253 mass spectrometer with the simultaneous collection of ion beams corresponding to masses 44-49 to obtain Δ₄₇, Δ₄₈, Δ₄₉, δ¹³C and δ¹⁸O values. The mass 47 beam is composed of ¹⁷O¹³C¹⁷O, ¹⁷O¹²C¹⁸O and predominantly ¹⁸O¹³C¹⁶O and we define R⁴⁷ as the abundance of mass 47 isotopologues divided by the mass 44 isotopologue. (R⁴⁷=[¹⁷O¹³C¹⁷O+¹⁷O¹²C¹⁸O+¹⁸O¹³C¹⁶O]/[¹⁶O¹²C¹⁶O].) Δ₄₇ is reported relative to a stochastic distribution of isotopologues for the same bulk isotopic composition. (Δ₄₇=(((R⁴⁷_{measured}/R⁴⁷_{stochastic})-1)-((R⁴⁶_{measured}/R⁴⁶_{stochastic})-1)-((R⁴⁵_{measured}/R⁴⁵_{stochastic})-1))*1000.) Masses 48 and 49 were monitored to detect any hydrocarbon contamination. Measurements of each gas consisted of 8–26 acquisitions, each of which involved 10 cycles of sample-standard comparison with an ion integration time of 20 s per cycle. Internal standard errors of this population of acquisition to acquisition for Δ₄₇ ranged from 0.005–0.01‰, (1–2°C) while external standard error ranged from 0.002–0.014‰ (0.4–2.7°C). The internal standard error for δ¹³C ranged from 0.5–1 ppm and the internal standard error for δ¹⁸O ranged from 1–3 ppm.

2.4 RESULTS

Table 2.1 summarizes results of isotopic analyses of all coral samples investigated in this study. A 0.16‰ range in Δ₄₇ was observed among coral samples having an estimated range in

growth temperature of 2–25°C (Table 2.1; Fig. 2.1). Table 2.1 also reports the $\delta^{18}\text{O}_{\text{PDB}}$ values of corals analyzed in this study, along with growth temperatures, and the $\delta^{18}\text{O}$ values of the water from which the corals grew. The $\delta^{18}\text{O}$ of the water from which the coral grew was reconstructed through a combination of the LEVITUS salinity database (<http://ingrid.ledo.columbia.edu/SOURCES/.LEVITUS94/.ANNUAL/.sal/>) and the NASA $\delta^{18}\text{O}$ of seawater database (<http://data.giss.nasa.gov/cgi-bin/o18data/geto18.cgi>). The LEVITUS database is more finely gridded for salinity than the NASA database. So we determined the relationship between $\delta^{18}\text{O}$ of the seawater and salinity near the sample site and used the salinity as determined by LEVITUS to calculate the $\delta^{18}\text{O}$ of the seawater from the $\delta^{18}\text{O}$ of the seawater vs. salinity relationship. The total error on the calculated $\delta^{18}\text{O}_{\text{sw}}$ calculated ranged from 0.1–0.2‰.

Figure 1 plots the Δ_{47} values of deep-sea corals vs. their nominal growth temperatures. The *Porites* surface coral BIR-1 has significant error bars in the temperature axis, unlike the deep-sea coral samples (where growth temperatures do not vary significantly seasonally), because it was collected in the Red Sea and sea surface temperatures range from 22–28°C through the year (Ghosh et al., 2006). Ghosh et al. (2006) found vital effects in the winter band of BIR-1. Our analyses are of one annual band that was crushed and homogenized, and we do not observe any offsets from equilibrium. This inconsistency could be because winter bands do not contribute a significant portion of the annual cycle.

The relationship of Δ_{47} to temperature is similar to that of inorganic precipitates. In a plot of Δ_{47} vs. $1/T^2$ the two species of solitary corals, *Desmophyllum* (slope: 0.0495 ± 0.012 ; intercept: 0.1052 ± 0.1557) and *Caryophyllum* (slope: 0.05545 ± 0.008 ; intercept: 0.0302 ± 0.1116) are indistinguishable in slope and intercept from the inorganic calibration line (slope: 0.0597 ± 0.004 ; intercept: -0.03112 ± 0.0475). Note, however, that these equations are not suitable for

Table 1

Name	Genus	$\delta^{13}\text{C}$	$\delta^{18}\text{O}_{\text{mineral}}$	Growth Temperature		error in Δ_{47}	$\delta^{18}\text{O}_{\text{w}}$
				(°C)	Δ_{47}		
47413	Desmophyllum	-5.009	0.723	7.9	0.733	0.007	-0.439
47413	Desmophyllum	-6.274	0.343	7.9	0.736	0.006	-0.439
47413	Desmophyllum	-4.877	0.686	7.9	0.732	0.009	-0.439
47413	Desmophyllum	-4.720	0.764	7.9	0.736	0.008	-0.439
47413	Desmophyllum	-6.285	-0.006	7.9	0.722	0.005	-0.439
47413	Desmophyllum	-4.544	0.833	7.9	0.726	0.007	-0.439
47413	Desmophyllum	-6.286	0.032	7.9	0.697	0.006	-0.439
80404	Desmophyllum	-1.230	1.535	13.1	0.707	0.009	0.25
80404	Desmophyllum	-1.826	1.764	13.1	0.695	0.008	0.25
80404	Desmophyllum	-1.185	1.611	13.1	0.717	0.010	0.25
47407	Desmophyllum	-5.640	0.768	4.2	0.749	0.006	-0.047
48738	Desmophyllum	-1.478	2.987	9.8	0.762	0.010	0.624
48738	Desmophyllum	-1.567	2.968	9.8	0.715	0.005	0.624
48738	Desmophyllum	-4.897	1.537	9.8	0.727	0.008	0.624
47409	Desmophyllum	-3.640	1.171	2.3	0.772	0.008	-0.088
62308	Desmophyllum	-4.725	1.147	3.7	0.744	0.010	0.5
77019	Ennallapsammia	-0.212	3.670	14.3	0.675	0.004	0.95
47531	Ennallapsammia	-1.603	0.982	7.5	0.738	0.009	-0.14
49020	Caryophyllia	0.708	1.548	17.4	0.688	0.011	0.907
45923	Caryophyllia	0.289	3.139	4.6	0.744	0.008	0.68
1010252	Caryophyllia	-0.115	2.818	6.1	0.744	0.008	0.222
BIR-1	Porites	-1.092	-3.720	25.2	0.650	0.006	1.91
BIR-2	Porites	-1.183	-3.670	25.2	0.639	0.006	1.91
BIR-3	Porites	-1.186	-3.659	25.2	0.648	0.005	1.91
BIR-4	Porites	-1.195	-3.664	25.2	0.615	0.007	1.91

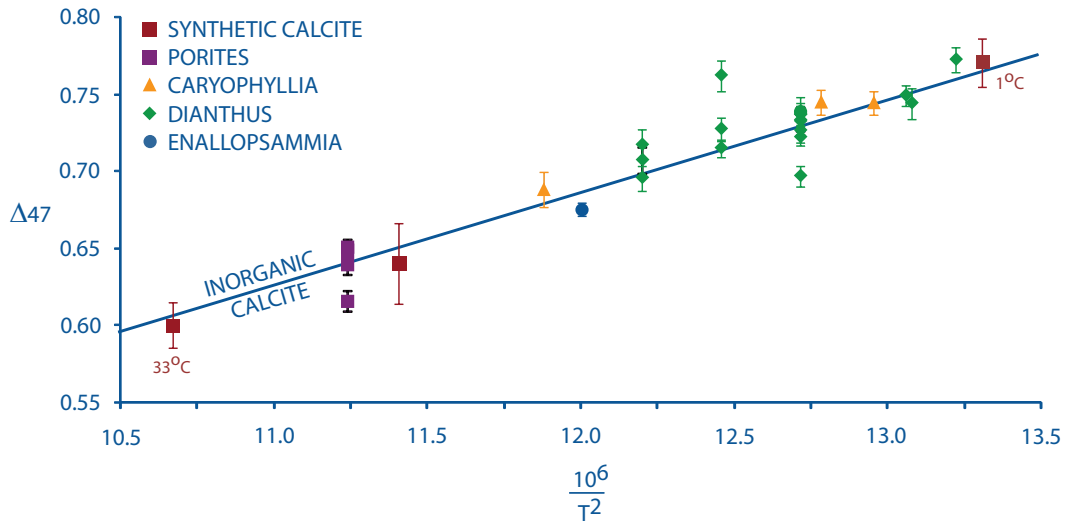


Figure 2.1: Clumped isotope calibratino of deep-sea corals and *Porites*, a surface coral. The dashed line is the inorganic calibration line as determined by measuring CO₂ produced from synthetic carbonates grown in the laboratory at known and controlled temperatures (Ghosh et al. 2006).

extrapolation beyond the range of observations (0–50°C).

2.4.i Internal and External Standard Errors

The average standard error for our Δ_{47} measurements are in agreement with the shot noise limit predicted for the analyses (Fig 2.2). Samples that were run for several hours have the lowest standard error, on the order of 0.005‰, which corresponds to a 1°C temperature change for low temperatures on the Ghosh et al. (2006) temperature scale. Several of the corals examined in this study were analyzed multiple times each, permitting us to estimate the external reproducibility for individual measurements of a given sample. This external standard error (i.e., the standard error of the average of multiple extractions) ranges from 0.005 to 0.014‰ (1–2.8°C), and decreases with the number of measurements (Fig 2.3). If one extraction of sample 47413 (a measurement we suspect was compromised by exchange of water) is excluded from these statistical calculations, the external standard error ranges from 0.002–0.014‰ (0.4–2.8°C). This external standard error is still larger than the expected shot noise errors for the same samples (~0.0025–0.0040‰). The difference in external standard error from expected shot noise limits may be due to sample heterogeneity, unaccounted for analytical fractionations, or contaminants in the sample.

The reproducibility we document has implications for future analyses of deep-sea corals. If sample size is limited, the best precision attainable is 0.005‰ ($\pm 1^\circ\text{C}$). However if sample size is not the limiting factor, the coral is homogenous, and not contaminated or otherwise analytically fractionated, precision is demonstrably as good as 0.002‰ ($\pm 0.4^\circ\text{C}$).

2.5. DISCUSSION

2.5.i Relationship of $\Delta 47$ to Temperature

For two of the solitary coral genera analyzed in this study, each exhibit slopes and in-

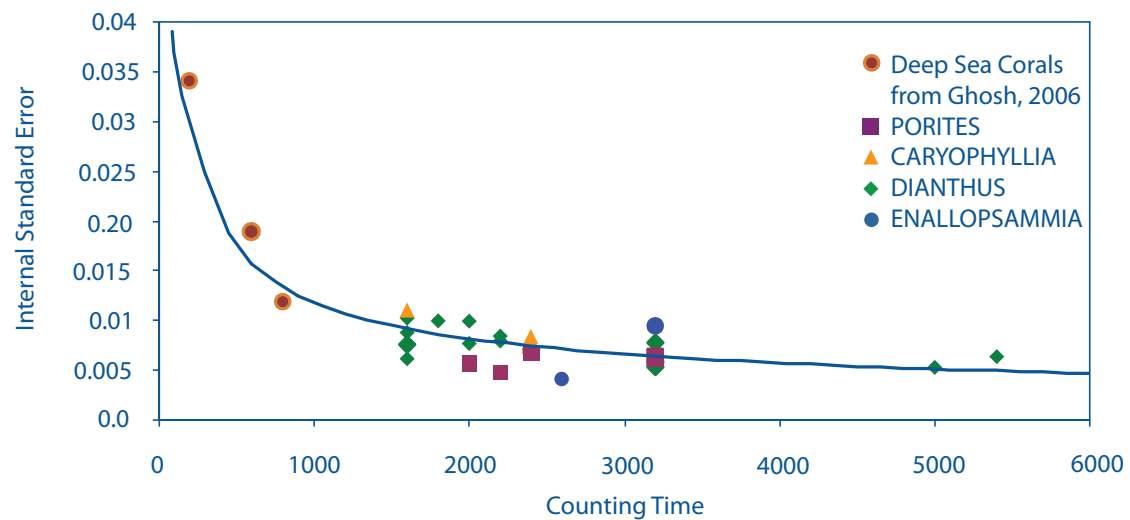


Figure 2.2: Internal standard error of our measurements with counting time. The dark line is the shot noise calculation. The error in our measurements is dominated by shot noise errors and decreases with increasing counting time.

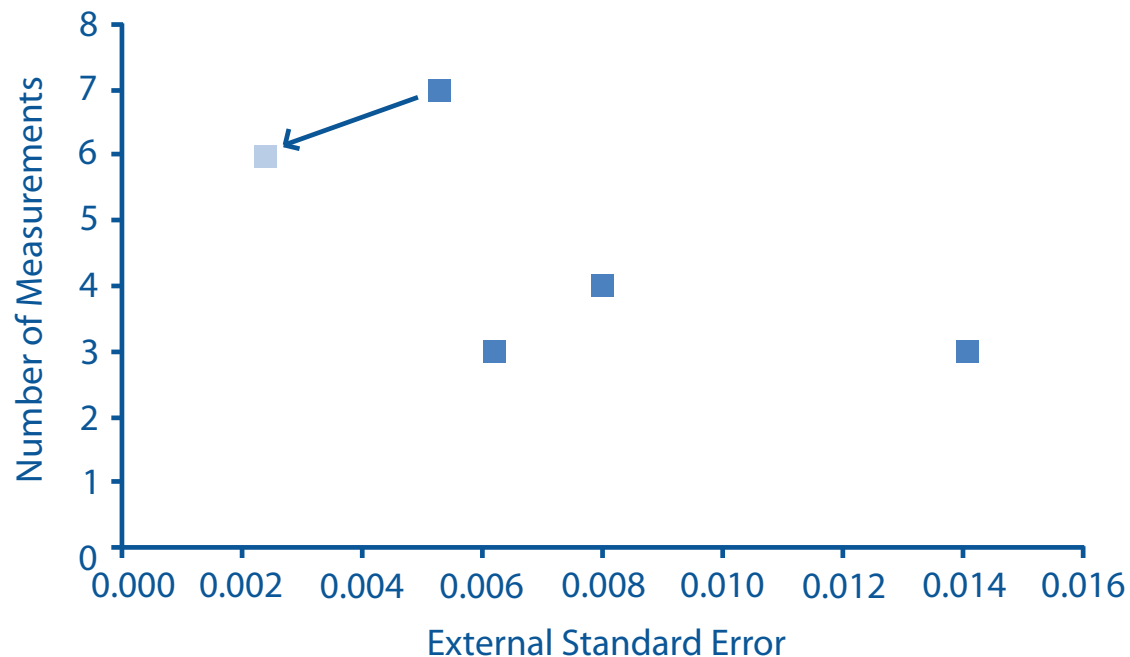


Figure 2.3: A figure of the external standard error of our measurements. Multiple replicates decreases the standard error of our measurements. The arrow indicates how coral 47413 changes if one extraction (suspected of having exchanged with water) is removed.

tercepts in a plot of Δ_{47} vs. $1/T^2$ that are within error of the inorganic calibration line (Fig 2.1).

Since the publication of the Ghosh et al. (2006) calibration, several more measurements have been made of inorganic calcite, foraminifera, mollusks, and soil carbonates having independently known growth temperatures. Most of these previous measurements are indistinguishable from the inorganic calibration line (Came et al., 2007; Daeron, 2007; Tripathi, 2007). There have however been nonequilibrium results obtained for speleothems and some synthetic carbonates (Affek et al., 2008; Guo, 2009). A recently published calibration for inorganic synthetic calcite (Dennis and Schrag, 2010) also disagrees with the Ghosh et al. (2006) result at low temperatures ($< \sim 15^\circ\text{C}$). The source of this discrepancy is unclear; it could reflect some combination of analytical artifacts (including intralaboratory calibration discrepancies) and/or kinetic isotope effects in carbonate synthesis reactions in either or both studies. We simply note here that this study presents data for 15 samples analyzed in this low temperature range, and they follow a temperature-dependence closely similar to that proposed by Ghosh et al. (2006), but steeper than that presented by Dennis and Schrag (2010). We suggest two straightforward explanations for this result: either the Ghosh et al. (2006) data reflect a kinetic isotope effect at low temperature that is mimicked by a vital effect in deep-sea corals (and, similarly, other classes of organisms previously observed to conform to the Ghosh et al. (2006) trend), yet independent of the vital effect on $\delta^{18}\text{O}$ and $\delta^{13}\text{C}$ in those corals (see below); or the Dennis and Schrag (2010) calibration is influenced by a kinetic isotope effect in low-temperature experiments. In the absence of any additional constraints, the second of these seems to us to be the more plausible explanation, and we will presume this for the rest of this discussion. But, we emphasize that inorganic calibrations will likely remain a subject of ongoing research and this interpretation should be revisited as new data come to light.

Three individual analyses made as part of this study are inconsistent with the inorganic

calcite calibration trend (i.e., differ from it by more than 2 sigma external error). Two of the outliers are an extraction from each of the samples 47413 and 48738. These outliers were extractions from corals that have been analyzed several times, and in both cases all other extractions from that sample exhibited no offset in Δ_{47} from the inorganic calibration line. Sample 47413 is unusual because, although the outlier was free of recognized contaminants, it did have a higher Δ_{47} and lower $\delta^{18}\text{O}$ than all the other replicates of that sample. This combination indicates that it could have exchanged with water (Pasadena tap water: 25°C, $\delta^{18}\text{O} = -8\text{\textperthousand}$) at some point during sample processing. Sample 48738 has an orange organic crust coating it, implying that perhaps it is not modern or that the organic coating was not completely removed prior to sample processing and affected the measurement. In any event, these two measurements are irreproducible exceptions to the otherwise straightforward trend produced by all other analyses, and thus we do not believe they indicate any systematic discrepancy between corals and inorganic calcite in Δ_{47} systematics. The third outlier is 77019, an *Enallopsammia* from 30°N, 76°W at 494 m of water depth in the core of the Gulf Stream, a region known for seasonal and interannual variations in salinity. This coral is also peculiarly enriched in $\delta^{18}\text{O}$ indicating possible uncertainties in the $\delta^{18}\text{O}_w$ reconstructed at this site.

The accuracy of deep-sea coral temperature estimates based on the calibration in Figure 2.1 will depend on uncertainties in both the Δ_{47} of the sample and uncertainties in the calibration line, whereas the precision of sample-to sample differences will depend only on the Δ_{47} measurements of samples. If one considers all previous measurements of published and unpublished inorganic and biogenic calibration materials (egg shells, teeth, otoliths, mollusks, brachiopods, corals and foraminifera; we exclude here the recent inorganic data of Dennis and Schrag (2010), discussed above) to be part of a single trend (i.e., because trends defined by each material are

statistically indistinguishable), then they make up a calibration line of slope in Δ_{47} vs. $1/T^2$ space of 0.0548 ± 0.0019 and intercept of -0.0303 ± 0.0221 . The standard error of the calibration is 0.0018% . If one excludes otoliths, which differ most from the other trends (perhaps due to a small vital effect, or due to inaccuracies in estimated body temperatures, or some other factor) and planktic foraminifera (where the variation in temperature with water depth and season is large and therefore a mean hard to estimate with confidence), the calibration line has a slope and intercept of 0.0562 ± 0.0020 and 0.0167 ± 0.0226 . The standard error in the calibration is then 0.0019% . The formal errors in slope and intercept of the overall calibration are trivially small; though one should not extrapolate the fitted trend outside of its range in calibration temperatures (particularly at higher temperatures, where the slope flattens considerably; (Dennis and Schrag 2010, Eiler, 2009). Thus, barring some unrecognized systematic error in all of the calibration data sets, the accuracy of temperature estimates of samples is dominated by error in the Δ_{47} measurement of the sample, which is generally dominated by shot noise error. The shot noise error for Δ_{47} analyses under normal analytical conditions generally levels off (ceases to improve with increased counting time) at $\sim 0.005\%$ (or $\sim 1^\circ\text{C}$) after 4500 seconds or ~ 20 acquisitions. Current analytical methods require 11 mg of CaCO_3 for 4500 seconds (i.e., to achieve 0.005% precision). If large amounts of homogeneous sample are available, precision could be improved further by combining data from multiple measurements of 11 mg sample aliquots. Sub degree precisions should be possible in this case. For example, if 11 mg of coral analyzed for 4500+ seconds resulted in a measurement of 2°C with a standard error of 0.005% , or 1°C , then six 11 mg measurements of the same homogeneous coral could result in a precision as low as 0.002% or 0.4°C (plus the small error in the accuracy of the calibration). Or, if three replicate measurements were made for the top of a deep-sea coral and six of the bottom of the same deep-sea coral

(i.e., if one were searching for evidence of temperature change over the course of its growth), the error in the temperature estimate at the top would be $\pm 0.4^{\circ}\text{C}$, the error in the temperature at the bottom would be $\pm 0.7^{\circ}\text{C}$, and the temperature difference ($\Delta T = \text{top temperature} - \text{bottom temperature}$) would have an error of ± 0.8 (because the two errors would be added in quadrature).

2.5.ii Vital Effects Mechanisms

2.5.ii.a Vital Effects in Corals

Use of deep-sea corals (and other biogenic carbonates) as a paleoceanographic archive is complicated by a set of biological processes commonly referred to as vital effects. Vital effects have been observed in aragonitic corals as offsets from equilibrium in stable isotope and metal/calcium ratios for a given temperature and other equilibrium conditions. Vital effects in corals and other organisms have also been noted to be dependent on growth rate, kinetics, pH, light and to the presence or absences of photosymbionts (Cohen et al., 2002; McConaughey, 1989; Reynaud et al., 2007; Rollion-Bard et al., 2003; Weber and Woodhead, 1970).

The range of vital effects in conventional, or ‘bulk’ stable isotope compositions seen in deep-sea corals is 7‰ in $\delta^{18}\text{O}$ and 12‰ in $\delta^{13}\text{C}$. In contrast, Δ_{47} values do not appear to exhibit any vital effects (i.e., they remain indistinguishable from the inorganic calibration across the full studied temperature range). The analytical method used to determine Δ_{47} values simultaneously generates $\delta^{13}\text{C}$ and $\delta^{18}\text{O}$ values for the sample; therefore, it is possible for us to evaluate the extent to which each analyzed sample expressed ‘vital effects’ in their O and C isotope compositions. A plot of $\Delta_{47\text{measured}} - \Delta_{47\text{expected}}$ vs $\delta^{18}\text{O}_{\text{measured}} - \delta^{18}\text{O}_{\text{expected}}$ does not show any correlated trends, and there are no systematic deviations in $\Delta_{47\text{measured}}$ from $\Delta_{47\text{expected}}$ even when there are clearly offsets in $\delta^{18}\text{O}$ (Fig 2.4). While our study was not designed to examine the mechanisms of vital effects, our results offer new constraints on this problem.

The following sections compare our results with the predictions one would make based on various previously proposed vital effect mechanisms.

2.5.ii.b Diffusion

Diffusion of CO₂ through a lipid bilayer or of different carbonate species across a foraminifer shell has been proposed as a part of different vital effect models (Adkins et al., 2003; Zeebe et al., 1999, Erez, 2003). While we do not have a first principle understanding of how this type of diffusion might affect the Δ_{47} value, we can use other types of well-known diffusion to inform this discussion. The kinetic theory of gases predicts that a gas that is diffused through a small aperture ('Knudsen diffusion') will be depleted in heavy isotopes relative to the residual gas it leaves behind. This behavior is described by the equation $R^j_{\text{diffused}} = R^j_{\text{residue}} (M^i/M^j)^{0.5}$ where R^j is the ratio of the concentration of isotopologue j to i and M is the mass.

Knudsen diffusion predicts that for a CO₂ population that has undergone diffusive fractionation, the diffused gas will be 11.2‰ lower in $\delta^{13}\text{C}$, and 22.2‰ lower in $\delta^{18}\text{O}$, but only 0.5‰ higher in Δ_{47} . This seemingly counterintuitive behavior is due to the nonlinear dependence of the stochastic abundances of mass-47 CO₂ isotopologues on the bulk isotopic composition (Eiler and Schauble, 2004). For natural isotopic compositions, the stochastic abundance increases more for an incremental change in $\delta^{13}\text{C}$ or $\delta^{18}\text{O}$ than does the vector that describes diffusive fractionation in $\delta^{13}\text{C}$, $\delta^{18}\text{O}$ and Δ_{47} space. Therefore, a diffused population of gas would be more depleted in $\delta^{13}\text{C}$ and $\delta^{18}\text{O}$ but higher than expected in Δ_{47} .

Similarly, gas phase inter diffusion where gas A diffuses through gas B is described by the relation $D_a'/D_a = \{(M_a + M_b)/(M_a M_b) \times (M'_a M_b)/(M'_a + M_b)^{0.5}\}$, where M_a is the mass of the diffusing molecule, M_b is the mass of the gas through which gas A is diffusing and the primes indicate the presence of a heavy isotope. The gas phase diffusion of CO₂ through air generates

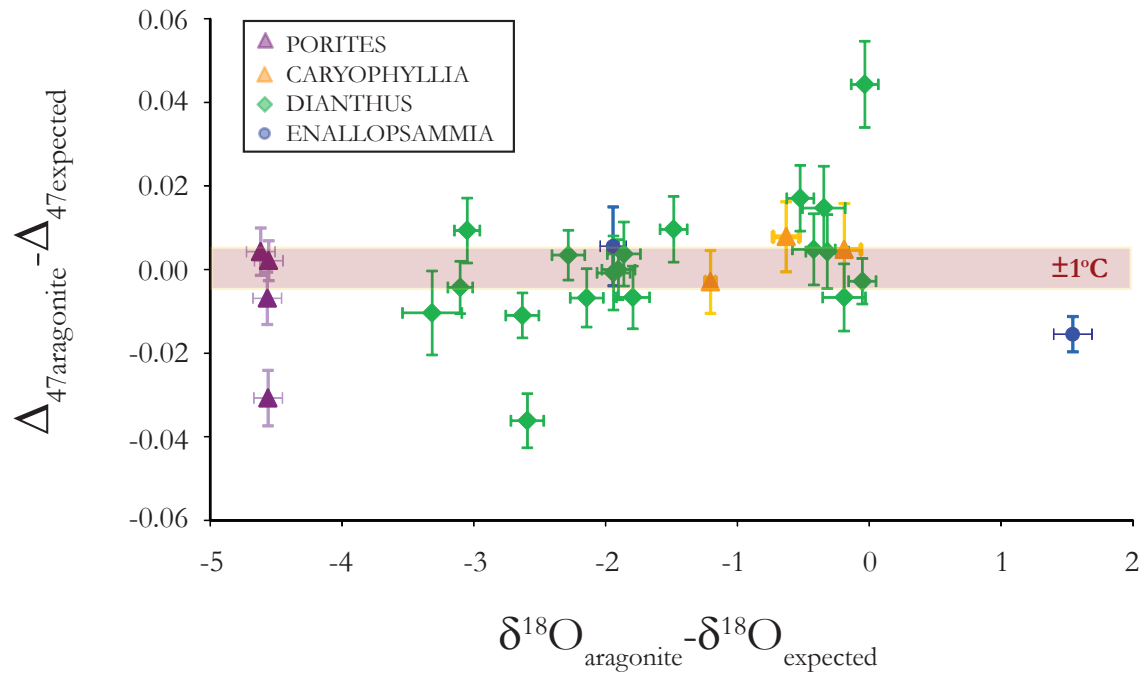


Figure 2.4: Offsets from equilibrium in Δ_{47} and $\delta^{18}\text{O}$. The biggest offsets in Δ_{47} are from corals with multiple extractions and every other extraction from those corals have no offset in Δ_{47} .

fractionations of -4.4‰ for $\delta^{13}\text{C}$, -8.7‰ for $\delta^{18}\text{O}$ and +0.3‰ for Δ_{47} . The enrichment of Δ_{47} in the diffused phase is again due to the relatively strong dependence of the stochastic abundance of mass-47 CO_2 on the bulk isotopic composition.

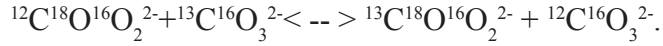
Isotopic fractionations caused by diffusion of molecules through a liquid medium are generally smaller than those associated with gas-phase diffusion. For instance, the ratio of diffusion coefficients of $^{12}\text{CO}_2$ and $^{13}\text{CO}_2$ in water is 1.0007 (O'Leary, 1984), whereas the gas phase interdiffusion equation, taking the medium to be H_2O predicts a fractionation factor of 1.0032. However, these condensed phase diffusive fractionations are generally described through a power-law relationship (i.e., the fractionation factor scales as the ratio of masses to some power, generally less than 0.5) (Bourg and Sposito, 2008). In this case, the mass dependence of the diffusive fractionation remains the same as for Knudsen diffusion, and the slope followed in a plot of Δ_{47} vs. $\delta^{18}\text{O}$ or $\delta^{13}\text{C}$ will remain the same. If so, then liquid phase diffusion of CO_2 should result in fractionations of -0.7‰ for $\delta^{13}\text{C}$ (i.e., the experimental constraint), -1.6‰ for $\delta^{18}\text{O}$ and +0.036‰ for Δ_{47} . On Figure 2.5 we have also indicated what 10% of the Knudsen and gas phase interdiffusion vector are to emphasize the difference between the scale of the different vectors. If deep-sea coral growth involved nonequilibrium isotopic fractionations that were dominated by diffusion across a lipid bilayer or in an aqueous medium, then a plot of Δ_{47} vs. $\delta^{18}\text{O}$ might have the same slope as the vectors that describe the types of diffusion discussed above. However the data is inconsistent with any of these predicted slopes (Fig 2.5). In addition, all of the diffusive processes predict $\delta^{13}\text{C}$ variations smaller than $\delta^{18}\text{O}$ variations, which is opposite to what is seen in deep-sea corals.

2.5.ii.c Mixing

The stochastic distribution that defines the reference frame for reporting Δ_{47} values has a

subtle saddle-shape curvature in a 3-dimensional plot of $\delta^{13}\text{C}$ vs. $\delta^{18}\text{O}$ vs. R^{47} . Therefore, conservative mixing of two CO_2 populations with the same Δ_{47} but different $\delta^{13}\text{C}$ and $\delta^{18}\text{O}$ leads to a mixed population having a different Δ_{47} value than the weighted sum of the Δ_{47} values of the end members (Eiler and Schauble, 2004).

Deep-sea corals have a large variation in $\delta^{13}\text{C}$ and $\delta^{18}\text{O}$ and could possibly produce Δ_{47} signals solely from this mixing effect. The range of variations seen in a single coral can be as large as 12‰ in $\delta^{13}\text{C}$ and 7‰ in $\delta^{18}\text{O}$ (Adkins et al., 2003). Two example end members seen in $\delta^{13}\text{C}$ and $\delta^{18}\text{O}$ are $\delta^{13}\text{C}=-10\text{\textperthousand}$ and $\delta^{18}\text{O}=-2\text{\textperthousand}$, and $\delta^{13}\text{C}=2\text{\textperthousand}$ and $\delta^{18}\text{O}=5\text{\textperthousand}$. If the stable isotopic variation in a deep-sea coral reflects variation in the DIC pool that the coral was using for calcification, we can calculate what magnitude of Δ_{47} offset would result from mixing between the isotopic end members of the DIC pool. However, the carbonate species of interest for calcification is not CO_2 (and its Δ_{47} value) but CO_3 and its corresponding $^{13}\text{C}-^{18}\text{O}$ clumped isotopologue. The relevant isotope exchange reaction for CO_3 species is:



So, we calculated the mixing effect on Δ_{63} (i.e., enrichment in mass-63 carbonate ion isotopologues, analogous to the Δ_{47} values of CO_2) and then converted this to a Δ_{47} value that would be measured in a coral skeleton. If both the high- and low- $\delta^{13}\text{C}$ and $\delta^{18}\text{O}$ share a common “ Δ_{63} ” value then we predict the amplitude of this mixing effect is as large as 0.02‰ for the case of 50% of each end member (which would generate the largest Δ_{63} offset, and still a relatively large offset in $\delta^{18}\text{O}$). Because phosphoric acid is believed to produce CO_2 having a Δ_{47} value that is offset by a constant amount from the Δ_{63} value of reactant carbonate (for a fixed temperature of reaction) this 0.02‰ enrichment due to mixing should be directly inherited by analyzed CO_2 (Guo et al., 2009). It is clear that this mixing model is inconsistent with the data, as there is no curvature to

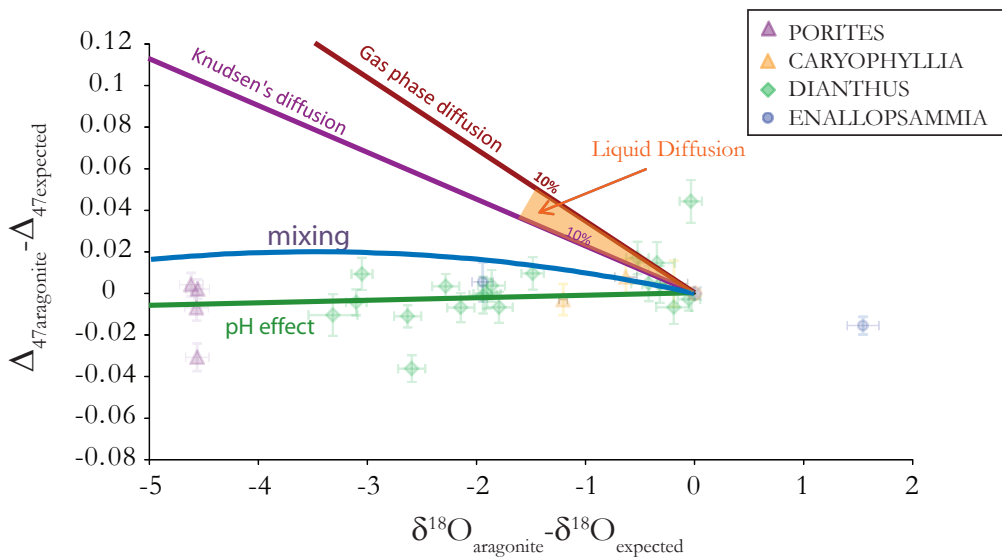


Figure 2.5: Vectors describing how various processes effect Δ_{47} and $\delta^{18}\text{O}$. Diffusive and mixing processes cannot explain the coupled variation in Δ_{47} and $\delta^{18}\text{O}$; however pH effects can.

the Δ_{47} vs. $\delta^{18}\text{O}$ trend unlike the mixing model (Figure 2.5). However, it is possible that mixing accompanied by re-equilibration would generate a horizontal line, and thus be more consistent with the data. Further experiments are needed to determine the rate that carbonate precipitating from DIC incorporates the different clumped carbonate species in DIC and whether mixing and subsequent re-equilibration would be recorded in the precipitating carbonates.

2.5.ii.d. pH

It has been demonstrated for inorganically precipitated carbonates that higher pH values (and thus higher CO_3^{2-} proportions in DIC) result in isotopically lower $\delta^{18}\text{O}$ values (McCrea, 1950; Usdowski et al., 1991). This observation has been explained by the pH dependent speciation of the DIC pool from which carbonate precipitates and the different fractionation factors between water and these DIC species. At seawater like pHs HCO_3^- dominates and at high pHs CO_3^{2-} dominates the DIC. McCrea (1950) and Usdowski et al. (1991) demonstrated that if calcium carbonate is quantitatively precipitated from a bicarbonate-carbonate solution, the oxygen isotopic composition of the solid reflects the weighted average of all the fractionation factors with respect to water for all the carbonate species. Zeebe (1999) exploited this observation to explain the variation seen in the inorganic carbonate data in Kim and O’Neil (1991) and existing stable oxygen isotope ratios of foraminiferal calcite.

It would be helpful to understand how the clumped isotope composition of the DIC varied with pH. Guo et al., (2008) theoretically estimated the Δ_{63} values of dissolved carbonate species in water; at 300K, CO_3^{2-} has a predicted value of 0.403‰, whereas HCO_3^- has a value of 0.421‰. While the absolute values of these calculated Δ_{63} estimates vary with the parameterization of the computational model, the offset between CO_3^{2-} and HCO_3^- remains constant at ~0.018‰, and thus is likely a robust feature of the calculation (Guo et al., 2008). The equivalent

difference in $\delta^{18}\text{O}$ at 19°C is 34.3‰ for HCO_3^- and 18.4‰ for CO_3^{2-} (Zeebe, 1999).

Given Zeebe's model of precipitation and Guo et al.'s (2008) calculated differences in Δ_{63} between HCO_3^- and CO_3^{2-} , we estimate the pH dependence of Δ_{63} of carbonate (which we take to be proportional to the measured Δ_{47} of CO_2 extracted from those carbonates). A change in pH from 7.9 to 9.8 leads to a change in CO_3^{2-} as a proportion of all DIC from 5% to 75% and a predicted change in Δ_{63} of carbonates by 0.0126‰ and in $\delta^{18}\text{O}$ of carbonates by 10.92‰. Thus, Zeebe's model predicts a slope of Δ_{47} vs. $\delta^{18}\text{O}$ measured in carbonate that closely approaches 0. However since the absolute values of the Δ_{63} estimates of the DIC species (and their relative difference to the calcium carbonate is unknown) the pH vector can only be plotted on Figure 2.5 with certain assumptions. Here we assume that when there is no offset in $\delta^{18}\text{O}$ from equilibrium, similarly there is no offset in Δ_{47} from the inorganic calibration line. That is, we are examining the sensitivity to pH not the absolute values of the Δ_{63} of the DIC species implied by different computational models. The resulting pH vector is consistent with our results (Fig 2.5).

2.5.ii.e Other Vital Effect Models

Watson (2004) proposed a model for near-surface kinetic controls on stable isotope compositions in calcite crystals, which also involves a sensitivity to DIC speciation. The model is based on the idea that the concentration of a particular trace-element in a crystal (which we could take to be an isotopologue of carbonate ion for our purposes) is primarily determined by two factors: the concentration of the element in the near-surface region of the crystal and the competition between crystal growth and ion migration in the near-surface region. There are three key regions, the specific growth surface which is a monolayer of atoms, the near-surface region and the bulk crystal lattice. The growth surface of the crystal could (due to its distinct structure) have an equilibrium composition that is different from that of the crystal lattice. Thus if the trace element

is selectively enriched (or depleted) on the growth surface, and if the diffusivity of that element in the near-surface region of the crystal is low, then the anomalous surface composition may be partially or completely preserved within the growth sector formed behind the growth surface. If however the diffusivity of the element in the near-surface region of the crystal is high, the newly formed crystal lattice is in equilibrium with the fluid it is growing from and has a different composition than the growth surface. Watson has explored this growth entrapment effect in various trace elements (Okorokov et al., 1996) and also extended it to oxygen isotopes (Watson, 2004). The Watson model identifies two potential sources of ^{18}O for calcite, CO_3^{2-} species alone or the weighted average of carbonate and bicarbonate ion (i.e., as in Zeebe's model). Carbonate ion is lower in $\delta^{18}\text{O}$ than solid carbonate when equilibrated with a common water. So, the Watson model predicts that if carbonate ion alone is added to growing solid carbonate, the solid will be lower than equilibrium for fast growth and approach equilibrium for slow growth. If instead both bicarbonate and carbonate ion contribute to solid, faster growth rates will be associated with higher-than equilibrium $\delta^{18}\text{O}$ values in the solid (because the higher $\delta^{18}\text{O}$ value of bicarbonate will be 'trapped' in the solid structure). It has been suggested that the $\delta^{18}\text{O}$ of aragonite decreases with increased growth rate in deep sea corals, based on textural variations of $\delta^{18}\text{O}$ within individual corals (Adkins et al., 2003). This observation is consistent with the Watson model for the case that carbonate ion alone contributes to the solid.

Clumped isotopes cannot yet be applied to the Watson model because there are several unknown factors. The Δ_{63} offset between $\text{CO}_3^{2-}(\text{aq})$ and $\text{CO}_3^{2-}(\text{s})$ is poorly known. The equilibrium partitioning in clumped isotopes between the fluid and the growth surface and the equilibrium partitioning between the fluid and the bulk crystal lattice is also unknown. The Δ_{63} of the CO_3^{2-} in aragonite is 0.430‰ (Schauble et al., 2006) while the Δ_{63} of HCO_3^- and CO_3^{2-} in DIC has

been predicted to be 0.421‰ and 0.403‰, respectively (Guo, 2009); however, because the Δ_{63} offset between CO_3 in water and CO_3 in aragonite is sensitive to the solvent model used to calculate the fractionation factors of the dissolved species (see above pH discussion), Guo's calculations of Δ_{63} cannot confidently be used to evaluate Watson's (2004) surface entrapment model. If however all these factors were known, then clumped isotopes could be a test for the Watson model.

McConaughey (1989) used the difference between symbiont bearing and nonsymbiont bearing aragonitic coral species from the same growth environment to constrain the chemical mechanisms behind vital effects. He determined that there is a kinetic effect and a metabolic effect fractionating oxygen and carbon isotopes in corals. The kinetic effect is due to the kinetic isotope effects (KIE) that occur during CO_2 hydration and hydroxylation. Therefore the linear variations seen in $\delta^{13}\text{C}$ and $\delta^{18}\text{O}$ are due to the incomplete isotopic equilibration of CaCO_3 and H_2O . Clumped isotopes cannot be used yet to evaluate McConaughey's kinetic fractionation model of stable isotope vital effects in corals as the KIE of CO_2 hydration and hydroxylation on clumped isotopes is currently unknown. However, if isotopic disequilibrium due to CO_2 hydration and hydroxylation is the dominant control of vital effects in corals then the magnitude of $\Delta_{47}/\delta^{18}\text{O}$ from this effect is constrained to be less than the observed variation in Figure 2.5. Rayleigh fractionation has also been proposed as a possible vital effects mechanism for the distribution of metals in corals (Cohen et al., 2006; Gagnon et al., 2007; Holcomb et al., 2009). This model assumes that there is an initial solution that is close to seawater composition which then undergoes closed system precipitation. Again clumped isotopes cannot yet be used to evaluate this vital effect mechanism as the partition coefficient of Δ_{47} for inorganic aragonite (where the partition coefficient is defined as: $D_{\text{arag}} \Delta_{47} = (\Delta_{47})_{\text{aragonite}} / (\Delta_{47})_{\text{seawater}}$) is unknown. The relevant

F, or extent of precipitation, is also unknown.

2.6 CONCLUSIONS

We present the relationship between the abundance of clumped isotopologues in CO₂ produced by phosphoric digestion of deep-sea corals and the coral's relationship to growth temperature. Deep-sea corals exhibit a temperature-dependent trend in Δ_{47} value that is indistinguishable in slope and intercept from inorganic calcite. This result indicates that deep sea corals can be used for paleothermometry, with precisions as good as $\sim 0.5^{\circ}\text{C}$. We also observe no vital effects in Δ_{47} for samples that display large vital effects in $\delta^{18}\text{O}$. This result is inconsistent with the predicted effects of diffusion or mixing for vital effects. However, pH effects could explain the observed variations in Δ_{47} and $\delta^{18}\text{O}$. In contrast to the results for Red Sea corals presented in Ghosh et al. (2006), we find no evidence of vital effects in surface corals. One of several possible explanations for this difference is that we analyzed mean annual bands rather than specific seasons (i.e., perhaps vital effects are specific only to relatively thin winter-growth bands in surface corals). Future work would involve a more detailed analysis of surface corals within annual bands to confirm the existence and determine the nature of any vital effect.

The degree-level errors in temperature in clumped isotope thermometry indicate that it is most suitable for thermocline and sea surface temperature studies, where temperature ranges are of order 10°C . However, sub degree precision is possible by averaging multiple replicates of homogeneous samples, making deep sea ocean temperatures studies (where temperature ranges are typically a few degrees) feasible.

Previous estimates of deep-sea temperature change across glacial/interglacial cycles have been made, using a combination of Mg/Ca ratios, or $\delta^{18}\text{O}_w$ with sea level curves. It is thought that in the deep Pacific the temperature changed 2°C , and the Atlantic changed by 4°C , between

MIS 5c and by 2°C (Cutler et al., 2003). Given the appropriate samples and sufficient effort at analytical replication, the clumped isotope thermometer should be able to further constrain glacial/interglacial temperature changes in the deep ocean.

References

Adkins, J. F., Boyle, E. A., Curry, W. B., and Lutringer, A., 2003. Stable isotopes in deep-sea corals and a new mechanism for “vital effects”. *Geochim Cosmochim Ac* 67, 1129–1143.

Adkins, J. F., McIntyre, K., and Schrag, D. P., 2002. The salinity, temperature, and d18O of the glacial deep ocean. *Science* 298, 1769–1773.

Affek, H. P., Bar-Matthews, M., Ayalon, A., Matthews, A., and Eiler, J. M., 2008. Glacial/interglacial temperature variations in Soreq cave speleothems as recorded by [']clumped isotope' thermometry. *Geochimica et Cosmochimica Acta* 72, 5351–5360.

Blunier, T. and Brook, E., 2001. Timing of millennial-scale climate change in Antarctica and Greenland during the last glacial period. *Science* 291, 109–112.

Bourg, I. C. and Sposito, G., 2008. Isotopic fractionation of noble gases by diffusion in liquid water: Molecular dynamics simulations and hydrologic applications. *Geochim Cosmochim Ac* 72, 2237–2247.

Cane, R. E., Eiler, J. M., Veizer, J., Azmy, K., Brand, U., and Weidman, C. R., 2007. Coupling of surface temperatures and atmospheric CO2 concentrations during the Palaeozoic era. *Nature* 449, 198–201.

Chappell, J. and Shackleton, N. J., 1986. Oxygen isotopes and sea level. *Nature* 324, 137-140.

Cohen, A., Owens, K. E., Layne, G., and Shimizu, N., 2002. The effect of algal symbionts on the accuracy of Sr/Ca paleotemperatures from coral. *Science* 296, 331–333.

Cohen, A. L., Gaetani, G. A., Lundalv, T., Corliss, B. H., and George, R. Y., 2006. Compositional variability in a cold-water scleractinian, *Lophelia pertusa*: new insights into “vital effects”. *Geochim Geophy Geosy* 7, doi:10.1029/2006GC001354.

Cutler, K. B., Edwards, R. L., Taylor, F. W., Cheng, H., Adkins, J., Gallup, C. D., Cutler, P. M.,

Burr, G. S., Chappell, J., and Bloom, A. L., 2003. Rapid sea-level fall and deep-ocean temperature change since the last interglacial. *Earth Planet Sc Lett* 206, 253–271.

Daeron, M., Quade, J., Eiler, J. 2007. Clumped-Isotope thermometry of modern pedogenic carbonates. *Agu Fall Meeting Abstracts*

Dennis, K. J. and Schrag, D. P., 2010. Clumped isotope thermometry of carbonatites as an indicator of diagenetic alteration. *Geochim Cosmochim Ac* 74, 4110–4122.

Eiler, J. A., Schable, E., and Kitchen, N., 2003. (Coo)-C-13-O-18-O-16 in Air. *Geochim Cosmochim Ac* 67, A86.

Eiler, J. M. and Schable, E., 2004. 18O13C16O in earth's atmosphere. *Geochimica et Cosmochimica Acta* 68, 4767–4777.

Eiler, J., Bonifacie, M., and Daeron, M, 2009. 'Clumped Isotope' Thermometry for High-Temperature Problems. *Geochimica et Cosmochimica Acta Conference Abstratcs*, A322.

Emiliani, C., 1955. Pleistocene temperatures. *Journal of Geology* 63, 538–578.

Emiliani, C., Hudson, J. H., Shinn, E., and George, R. Y., 1978. Oxygen and carbon isotopic growth record in a reef coral from the Florida Keys and a deep-sea coral from Blake Plateau. *Science* 202, 627–629.

Epstein, S., Buchsbaum, R., Lowenstam, H. A., and Urey, H. C., 1953. Revised carbonate-water isotopic temperature scale. *Geol. Soc. Amer. Bull.* 64, 1315–1326.

Gagnon, A. C., Adkins, J. F., Fernandez, D. P., and Robinson, L. F., 2007. Sr/Ca and Mg/Ca vital effects correlated with skeletal architecture in a scleractinian deep-sea coral and the role of Rayleigh fractionation. *Earth Planet Sc Lett* 261, 280–295.

Ghosh, P., Adkins, J. F., Affek, H., Balta, B., Guo, W., Schable, E. A., Schrag, D. P., and Eiler, J. M., 2006. 13C-18O bonds in carbonate minerals: A new kind of paleothermometer. *Geochimica*

et *Cosmochimica Acta* 70, 1439–1456.

Guo, W., 2009. Carbonate Clumped Isotope Thermometry: Application to Carbonaceous Chondrites & Effects of Kinetic Isotope Fractionation, California Institute of Technology.

Guo, W., Daeron, M., Niles, P., Genty, D., Kim, S. T., Vonhof, H., Affek, H., Wainer, K., Blamart, D., and Eiler, J., 2008. C-13-O-18 bonds in dissolved inorganic carbon: Implications for carbonate clumped isotope thermometry. *Geochim Cosmochim Ac* 72, A336–A336.

Guo, W., Mosenfelder, J. L., Goddard Iii, W. A., and Eiler, J. M., 2009. Isotopic fractionations associated with phosphoric acid digestion of carbonate minerals: Insights from first-principles theoretical modeling and clumped isotope measurements. *Geochim Cosmochim Ac* 73, 7203–7225.

Holcomb, M., Cohen, A. L., Gabitov, R. I., and Hutter, J. L., 2009. Compositional and morphological features of aragonite precipitated experimentally from seawater and biogenically by corals. *Geochim Cosmochim Ac* 73, 4166–4179.

Kim S.-T. and O’Neil J. R. (1997) Equilibrium and nonequilibrium oxygen isotope effects in synthetic carbonates. *Geochim. Cosmochim. Acta* 61, 3461–3475.

McConaughay, T., 1989. ^{13}C and ^{18}O isotopic disequilibrium in biological carbonates: I. Patterns. *Geochim Cosmochim Ac* 53, 151–162.

McCrea, J. M., 1950. On the isotopic chemistry of carbonates and a paleotemperature scale. *Journal of Chemical Physics* 18, 849–857.

O’Leary, M. H., 1984. Measurement of the isotope fractionation associated with diffusion of carbon dioxide in aqueous solution. *The Journal of Physical Chemistry* 88, 823–825.

Okorokov, A. L., Panov, K. I., Kolbanovskaya, E. Y., Karpeisky, M. Y., Polyakov, K. M., Wilkinson, A. J., Dodson, G. G., and Watson, E. B., 1996. Surface enrichment and trace-element uptake

during crystal growth. *Geochim Cosmochim Ac* 60, 5013–5020.

Reynaud, S., Ferrier-Pagès, C., Meibom, A., Mostefaoui, S., Mortlock, R., Fairbanks, R., and Allemand, D., 2007. Light and temperature effects on Sr/Ca and Mg/Ca ratios in the scleractinian coral *Acropora* sp. *Geochim Cosmochim Ac* 71, 354–362.

Rollion-Bard, C., Chaussidon, M., and France-Lanord, C., 2003. pH control on oxygen isotopic composition of symbiotic corals. *Earth Planet Sc Lett* 215, 275–288.

Schauble, E. A., Ghosh, P., and Eiler, J. M., 2006. Preferential formation of ^{13}C - ^{18}O bonds in carbonate minerals, estimated using first-principles lattice dynamics. *Geochim Cosmochim Ac* 70, 2510–2529.

Schrag, D. P. and DePaolo, D. J., 1993. Determination of $\delta^{18}\text{O}$ of seawater in the deep ocean during the Last Glacial Maximum. *Paleoceanography* 8, 1–6.

Shackleton, N. J., 1967. Oxygen isotope analyses and Pleistocene temperatures re-assessed. *Nature* 215, 15–17.

Tripathi, A. a. T., N. and Eiler, J., 2007. Carbonate ‘clumped isotope’ thermometry in planktonic foraminifera and coccoliths. *AGU Fall Meeting Abstracts*, B1263.

Urey, H. C., 1947. The thermodynamic properties of isotopic substances. *J. Chem. Soc.* 1947, 562–581.

Usdowski, E., Michaelis, J., Bottcher, M. E., and Hoefs, J., 1991. Factors for the oxygen isotope equilibrium fractionation between aqueous and gaseous CO_2 , carbonic acid, bicarbonate, carbonate, and water (19°C). *Zeitschrift fur Physikalische Chemie* 170, 237–249.

Watson, E. B., 2004. A conceptual model for near-surface kinetic controls on the trace-element and stable isotope composition of abiogenic calcite crystals. *Geochimica et Cosmochimica Acta* 68, 1473–1488.

Weber, J. N. and Woodhead, P. M. J., 1970. Carbon and oxygen isotope fractionation in the skeletal carbonate of reef-building corals. *Chem Geol* 6, 93–117.

Weber, J. N., 1973. Deep-sea ahermatypic scleratinian corals: isotopic composition of the skeleton. *Deep-Sea Research* 20, 901–909.

Zeebe, R., 1999. An explanation of the effect of seawater carbonate concentration on foraminiferal oxygen isotopes. *Geochim Cosmochim Ac* 63, 2001–2007.

Zeebe, R. E., Bijma, J., and Wolf-Gladrow, D. A., 1999. A diffusion-reaction model of carbon isotope fractionation in foraminifera. *Marine Chemistry* 64, 199–227.